
LIKELIHOOD REGRET: AN OUT-OF-DISTRIBUTION DETECTION SCORE FOR VARIATIONAL AUTO-ENCODER

A PREPRINT

Zhisheng Xiao *
Computational and Applied Mathematics
University of Chicago
Chicago, IL, 60637
zxiao@uchicago.edu

Qing Yan *
Department of Statistics
University of Chicago
Chicago, IL, 60637
yanq@uchicago.edu

Yai Amit
Department of Statistics
University of Chicago
Chicago, IL, 60637
amit@marx.uchicago.edu

February 22, 2021

ABSTRACT

Deep probabilistic generative models enable modeling the likelihoods of very high dimensional data. An important application of generative modeling should be the ability to detect out-of-distribution (OOD) samples by setting a threshold on the likelihood. However, a recent study shows that probabilistic generative models can, in some cases, assign higher likelihoods on certain types of OOD samples, making the OOD detection rules based on likelihood threshold problematic. To address this issue, several OOD detection methods have been proposed for deep generative models. In this paper, we make the observation that some of these methods fail when applied to generative models based on Variational Auto-encoders (VAE). As an alternative, we propose Likelihood Regret, an efficient OOD score for VAEs. We benchmark our proposed method over existing approaches, and empirical results suggest that our method obtains the best overall OOD detection performances compared with other OOD method applied on VAE.

1 Introduction

In order to make reliable and safe decisions, deep learning models that are deployed for real life applications need to be able identify whether the input data is anomalous or significantly different from the training data. Such data are called out-of-distribution (OOD) data. However, it is known that neural network classifiers can over-confidently classify OOD data into one of the training categories [26]. This observation poses a great challenge to the reliability and safety of AI [1], making OOD detection a problem of primary importance. Several approaches have been proposed to detect OOD data based on deep classifiers [9, 15, 5, 10]. Unfortunately, these methods cannot be applied to OOD detection for models trained without supervision. An appealing alternative that works for unsupervised OOD detection is to use probabilistic generative models that approximate the true distribution of the training data. Such models can evaluate the likelihood of input data, and if a generative model fits the training data distribution well enough, it should assign high likelihood to samples from the training distribution and low likelihood to OOD samples. As a consequence, it is believed that a threshold on likelihood can be a good OOD detector.

Recent advances in deep probabilistic generative models [11, 35, 31, 12] make generative modeling of very high dimensional and complicated data such as natural images, sequences [27] and graphs [13] possible. These models can evaluate the likelihood of input data easily and generate realistic samples, indicating that they approximate the distribution of training data well. Therefore, it would appear promising to use deep generative models to detect OOD data [17]. However, some recent studies [23, 4] reveal a counter intuitive phenomenon that challenges the validity of unsupervised OOD detection using generative models. They observe that likelihoods obtained from current state-of-the-art deep probabilistic generative models fail to distinguish between training data and some obvious OOD input types that are easily recognizable by humans. For example, [23] shows that generative models trained on CIFAR-10 output

*equal contribution

higher likelihood on SVHN than on CIFAR-10 itself, despite the fact that images in CIFAR-10 (contains dogs, trucks, horses, etc.) and SVHN (contains street house numbers) have very different semantics.

At this point, no effective method has been discovered to ensure that these generative models make the correct likelihood assignment on OOD data. Alternatively, some new metrics based on likelihood are proposed to alleviate this issue [29, 24, 32]. The OOD detection is performed by setting thresholds on the new metrics rather than on likelihoods. Some of these works report impressive OOD detection performances on invertible flow-based models [12] and auto-regressive models [31]. Interestingly, we observe that these scores can be much less effective for Variational Auto-encoders (VAE), an important type of probabilistic generative models. Previously, VAE is wide used for anomaly detection, and empirical successes are achieved in the web applications [37], time series [38]. However, the failure of current OOD scores on VAE suggests that a new score is necessary. To this end, in this paper we propose a simple yet effective metric called Likelihood Regret (LR) to detect OOD samples with VAE. The Likelihood Regret of a single input can be interpreted as the ratio between its likelihood as approximated by the VAE, and the likelihood obtained by the optimal posterior distribution for that input. We conduct comprehensive experiments to evaluate our proposed metric on a variety of image OOD detection tasks with VAE, and we show that it obtains the best overall performances.

The contributions of this paper can be summarized as follows:

- We make the important observation that some recent OOD detection scores for generative models may fail on VAE and we present empirical results confirming this fact.
- We propose Likelihood Regret, a new score for OOD detection with VAE and we show the effectiveness of our metric through evaluations on image OOD detection tasks.

2 Background

In this section, we include some background on VAEs focusing on topics related to this paper. We also include background on OOD detection with generative models.

2.1 Variational Auto-Encoder

VAE [11, 30] is an important type of deep probabilistic generative model with many practical applications [18, 19, 8]. It uses a latent variable \mathbf{z} with prior $p(\mathbf{z})$, and a conditional distribution $p_\eta(\mathbf{x}|\mathbf{z})$, to model the observed variable \mathbf{x} . The generative model, denoted by $p_\theta(\mathbf{x})$, can be formulated as $p_\theta(\mathbf{x}) = \int_{\mathbf{z}} p_\eta(\mathbf{x}|\mathbf{z})p(\mathbf{z})d\mathbf{z}$. However, direct computation of this likelihood is intractable in high dimensions, so variational inference is used to derive a lower bound on the log likelihood of \mathbf{x} . This leads to the famous evidence lower bound (ELBO):

$$\begin{aligned} \log p_\theta(\mathbf{x}) &\geq \log p_\theta(\mathbf{x}) - D_{\text{KL}}[q_\phi(\mathbf{z}|\mathbf{x})||p_\theta(\mathbf{z}|\mathbf{x})] \\ &= \mathbb{E}_{q_\phi(\mathbf{z}|\mathbf{x})}[\log p_\eta(\mathbf{x}|\mathbf{z})] - D_{\text{KL}}[q_\phi(\mathbf{z}|\mathbf{x})||p(\mathbf{z})] \\ &\triangleq \mathcal{L}(\mathbf{x}; \eta, \phi), \end{aligned} \tag{1}$$

where $q_\phi(\mathbf{z}|\mathbf{x})$ is the variational approximation to the true posterior distribution $p_\theta(\mathbf{z}|\mathbf{x})$. Both $q_\phi(\mathbf{z}|\mathbf{x})$ and $p_\eta(\mathbf{x}|\mathbf{z})$ are parameterized by neural networks with parameters ϕ (encoder) and η (decoder), respectively. The first term in ELBO is the reconstruction loss of \mathbf{x} , and the second term is the Kullback Leibler (KL) divergence between the variational posterior distribution and the prior. The VAE is trained by maximizing $\mathcal{L}(\mathbf{x}; \eta, \phi)$ over the training data.

Unlike generative models using exact inference where the likelihood can be directly computed, VAE only outputs a lower bound of log likelihood and the exact log likelihood needs to be estimated, usually by an importance weighted lower bound [3]:

$$\log p_\theta(\mathbf{x}) \geq \mathbb{E}_{\mathbf{z}^1, \dots, \mathbf{z}^K \sim q_\phi(\mathbf{z}|\mathbf{x})} \left[\log \frac{1}{K} \sum_{k=1}^K \frac{p_\eta(\mathbf{x}|\mathbf{z}^k) p(\mathbf{z}^k)}{q_\phi(\mathbf{z}^k|\mathbf{x})} \right] \triangleq \mathcal{L}_K(\mathbf{x}; \eta, \phi), \tag{2}$$

where each \mathbf{z}^k is a sample from the variational posterior $q_\phi(\mathbf{z}|\mathbf{x})$. It is proven in [3] that the inequality in (2) is asymptotically tight as K increases, therefore $\mathcal{L}_K(\mathbf{x}; \eta, \phi)$ is a good estimation for $\log p_\theta(\mathbf{x})$ when K is large. Throughout the paper, we use $K = 10000$ to estimate the log likelihood of a given input.

While the prior $p(\mathbf{z})$ and the variational posterior $q_\phi(\mathbf{z}|\mathbf{x})$ are often chosen to be Gaussians, there are multiple choices for the decoding distribution $p_\eta(\mathbf{x}|\mathbf{z})$ depending on the type of data. In this paper, we follow the settings of VAE experiments in [23] and choose the decoding distribution to be an independent 256-way categorical distribution (corresponding to 8-bit image data) on each pixel. Note that the same data distribution is also assumed by the PixelCNN model [35].

2.2 Problems of OOD Detection with Probabilistic Generative Models

Suppose we have a set of N training samples $\{\mathbf{x}_i\}_{i=1}^N$ drawn from some underlying data distribution $\mathbf{x}_i \sim p(\mathbf{x})$. Our goal is to decide whether a test sample \mathbf{x} is OOD, which, by definition in [9], means that \mathbf{x} has low density under $p(\mathbf{x})$. Probabilistic generative models $p_\theta(x)$ are trained on the set of training samples by maximizing the likelihood (or lower bound of likelihood). It is well known that maximizing the likelihood $p_\theta(\mathbf{x})$ is equivalent to minimizing $D_{\text{KL}}[p(\mathbf{x})\|p_\theta(\mathbf{x})]$, and thus a well trained generative model provides a good approximation to the true data distribution $p(\mathbf{x})$. Therefore, OOD data should have low likelihood under $p_\theta(\mathbf{x})$.

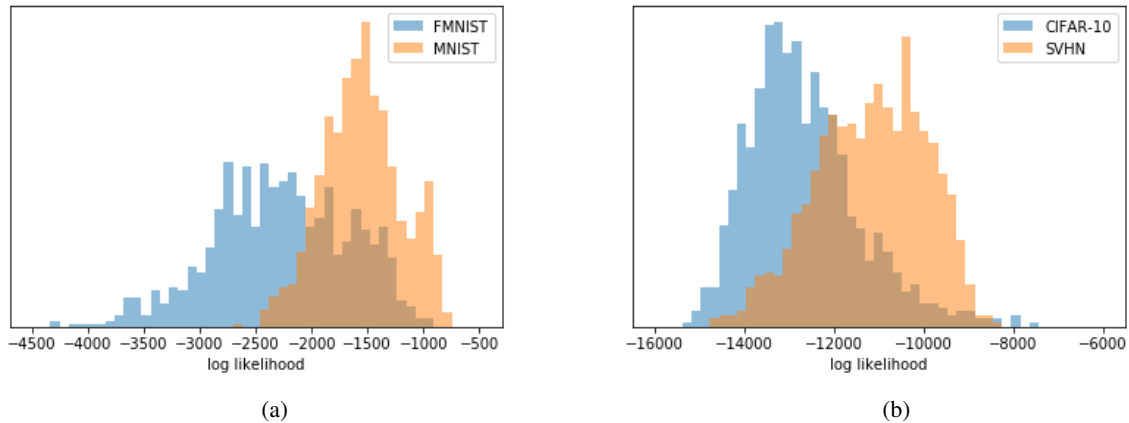


Figure 2.1: Histogram that compares the log likelihood of test samples from (a): Fshion MNIST and MNIST on a VAE trained on Fashion MNIST, and (b): CIFAR-10 and SVHN on a VAE trained on CIFAR-10. Both experiments show that VAEs may assign high likelihoods to OOD samples.

However, the above argument fails in practice, as noted in [23, 4]. In particular, [23] observe that almost all major types of probabilistic generative models, including VAE, flow-based model and auto-regressive model, can assign spuriously high likelihood to OOD samples. In Figure 2.1, we confirm that such a likelihood misalignment does exist on VAE, which is the model we focus on in this paper. We further observe that VAEs obtain surprisingly good reconstruction quality on OOD data (Figure 2.2), indicating that they model OOD samples very well. These observations suggest that VAEs do not really regard some samples from completely different distributions as OOD, and it is extremely unreliable to use likelihood as an OOD detector.



Figure 2.2: For each subfigure, the top row contains original images and the bottom row contains the reconstructed images. (a), (b): reconstruction of Fashion MNIST and MNIST images by amodel trained on Fashion MNIST. (c), (d): reconstruction of CIFAR-10 and SVHN images by a model trained on CIFAR-10.

3 Related Work

Since [23, 4] made the observation that probabilistic generative models may assign high likelihoods to OOD data, there have been intense discussions on how to alleviate this issue. One line of work is trying to train generative models that correctly assign low likelihoods to OOD samples. [7] show that energy-based models do not suffer seriously from the likelihood misalignment issue. However, the test likelihoods of in-distribution and OOD samples still exhibit

significant overlap, and more importantly, EBMs are known to be very hard to train. [2] train normalizing flows with an information bottleneck constraint and show some improvements on OOD detection, but the training requires labels, which contradicts the setting of unsupervised OOD detection. [21] propose bidirectional-inference VAEs with very deep hierarchy of latent variables and shows that if some levels of latent variables are replaced by samples from the prior during testing, the likelihood misalignment issue can be alleviated. However, this comes at the cost of much worse likelihood values, and the OOD detection performances are still not impressive. Note that all methods mentioned above do not apply to commonly used generative models under the settings in [23].

To the best of our knowledge, there is no consistent way to train generative models that can effectively detect OOD samples only by looking at likelihood, and therefore people seek to design new OOD scores. [4] observe that OOD samples have higher variance likelihood estimates under different independently trained models. Although the metric obtained from ensemble of models performs well, training multiple models can be very computationally expensive. [24] propose an explicit test of typicality, which involves a Monte Carlo estimate for the empirical entropy. [34] propose a new method for OOD detection that leverages batch normalization. However, both [24, 34] can only determine whether a *batch* of samples is an outlier or not, which greatly limits their applications to the real OOD detection task, where normally we want to detect if a single sample is in- or out-of-distribution.

Perhaps [29, 32] have the closest connection with our work. [29] propose the use of likelihood-ratio tests for OOD detection. Besides training a usual generative model, they also train a background model on random surrogates of input data. The likelihood ratio is obtained from taking the ratio between likelihoods of original model and background model. [32] hypothesizes that the likelihood of generative models are biased by the complexity of the corresponding inputs, and they offset the bias by a factor that measures the complexity of images. They use the length of lossless compression of the image as the complexity factor, and their OOD score can also be interpreted as a likelihood-ratio test statistic by regarding the compressor as a universal model. Our method is related in the sense that we share a likelihood ratio interpretation. [29, 32] obtain great OOD detection performances with Glow and Pixel-CNN, however, neither of them evaluates their methods on VAE. Later in this paper, we will show that their OOD scores do not work well with VAE, suggesting the need to design an effective OOD score for VAE.

4 Likelihood Regret for OOD Detection using VAEs

4.1 On the Necessity of New OOD Score for VAE

Before introducing our method, we would like to emphasize why it is necessary to design a metric of OOD detection for VAE. One might ask that given that OOD scores like [29, 32] work so well for Glow and PixelCNN, why not just apply them to VAEs? We point out a key difference between VAE and other generative models in Table 1, where we trained different generative models on Fashion MNIST and CIFAR-10 and report the test bits-per-dimension (BPD) of different datasets. The BPD is computed by normalizing the negative log likelihood by the dimension of an input: $\text{BPD}(\mathbf{x}) = \frac{-\log p_{\theta}(\mathbf{x})}{\log(2) \cdot d}$. We observe that while all generative models exhibit similar behavior of assigning high likelihoods to certain type of OOD samples, the relative changes in average likelihood across different datasets are distinct. In particular, the average test likelihood of VAE across different datasets have a much smaller range than that of Glow and PixelCNN, suggesting that the likelihoods of in-distribution and OOD samples are much less "separated away" in VAE. The reason is probably that flow-based and auto-regressive models try to model each pixel of the input image, while the bottleneck structure in VAE forces the model to ignore some information.

Less separated likelihoods of in-distribution and OOD samples make OOD detection for VAE harder, as some OOD scores rely on the gap of likelihoods. We will empirically show in Section 5 that current state-of-the-art generative model OOD scores are much less effective for VAE, partly due to the smaller gap of likelihoods. This suggests the need for a new OOD score for VAEs.

4.2 Our Proposed Metric

In this section we introduce Likelihood Regret (LR), our proposed OOD score. We present the computation of LR in Algorithm 1, and we provide detailed explanation below.

Suppose we have a VAE with encoder E_{ϕ} and decoder D_{η} . The ELBO objective (1) is indeed a function of the input \mathbf{x} , the parameters of the variational posterior distribution (which are the outputs of the encoder $E_{\phi}(\mathbf{x})$), and the decoder with parameters η . As commonly used in VAE [11], $q_{\phi}(z|x) \sim \mathcal{N}(\mu_x, \sigma_x^2 \mathbf{I})$, so the encoder outputs the mean and variance: $E_{\phi}(\mathbf{x}) = (\mu_x, \sigma_x)$. For clarity, we use τ to denote the sufficient statistics (μ, σ) for an isotropic Normal distribution, while $\tau(x, \phi)$ represents the values returned by encoder $E_{\phi}(x)$. Further we express

	VAE	Glow	PixelCNN		VAE	Glow	PixelCNN
FMNIST	3.20	3.25	2.68	CIFAR-10	4.12	4.05	3.57
MNIST	2.18	2.10	1.51	SVHN	3.63	2.65	2.39
Constant	4.21	1.35	4.01	Constant	2.49	0.76	0.85
Noise	8.89	8.96	7.71	Noise	5.98	9.38	10.17

(a) Trained on Fashion MNIST

(b) Trained on CIFAR-10

Table 1: Average BPD of different test datasets for VAE, Glow and PixelCNN trained on Fashion MNIST and CIFAR-10. The Noise data consist of images with independent sample from $\text{unif}[0, 1]$ on each pixel. The Constant data consist of random constant images where the constant is sampled from $\text{unif}[0, 0.1]$.

Algorithm 1 Computing Likelihood Regret (LR)

Input: Test sample \mathbf{x} , trained VAE (E_{ϕ^*}, D_{η^*}) , number of posterior samples for likelihood estimation K , number of optimization step S , learning rate γ .

- 1: $L_{\text{VAE}} = \mathcal{L}_K(\mathbf{x}; \eta^*, \phi^*)$ ▷ Estimate the log likelihood of \mathbf{x} under the VAE model by (2)
- 2: Set $\phi = \phi^*$
- 3: **for** S iterations **do**
- 4: $\phi \leftarrow \text{Adam}(\phi, \nabla_{\phi}(-\mathcal{L}(\mathbf{x}; \eta^*, \phi)), \gamma)$ ▷ Optimize ϕ by maximizing the ELBO objective
- 5: $L_{\text{OPT}} = \mathcal{L}_K(\mathbf{x}; \eta^*, \phi)$ ▷ Estimate the log likelihood of \mathbf{x} with optimized encoder
- 6: $\text{LR} = L_{\text{OPT}} - L_{\text{VAE}}$

ELBO in (1) as $\mathcal{L}(\mathbf{x}; \eta, \tau(\mathbf{x}, \phi))$ to emphasize its direct dependency on $\tau(\mathbf{x}, \phi)$. During training, based on empirical risk minimization (ERM) criterion, our objective is to obtain network parameters $\theta^* = (\phi^*, \eta^*)$ that maximize the population log likelihood $\log p_{\theta}(\mathbf{x})$:

$$(\phi^*, \eta^*) = \underset{\theta: (\phi, \eta)}{\text{argmax}} \frac{1}{n} \sum_{i=1}^n \log p_{\theta}(\mathbf{x}_i). \quad (3)$$

In other words, $\theta^* = (\phi^*, \eta^*)$ are the parameters that achieve best *average* log likelihood over the finite training set. In practice, we train VAE by maximizing ELBO instead of log likelihood. Since ELBO is a lower bound of log likelihood, we can regard maximizing ELBO as a good surrogate to maximizing log likelihood, so

$$(\phi^*, \eta^*) \approx \underset{(\phi, \eta)}{\text{argmax}} \frac{1}{n} \sum_{i=1}^n \mathcal{L}(\mathbf{x}_i; \eta, \tau(\mathbf{x}_i, \phi)). \quad (4)$$

Since $q_{\phi}(z|x)$ can be fully determined by $\tau(x, \phi)$, we also denote $\theta = (\eta, \tau)$ or $\theta = (\eta, \tau(\cdot, \phi))$ as an abuse of notation.

For a specific test input \mathbf{x} , we can fix the decoder parameters η^* , and find the optimal configuration of variational posterior distribution parameter $\hat{\tau}(\mathbf{x}) = (\hat{\mu}_x, \hat{\sigma}_x)$ that maximizes its *individual* log likelihood:

$$\hat{\tau}(\mathbf{x}) = \underset{\tau}{\text{argmax}} \{\log p_{\theta}(\mathbf{x}) | \theta = (\eta^*, \tau)\}. \quad (5)$$

In other words, $\hat{\tau}(x)$ is the optimal posterior distribution of latent variable z given an input x and the optimal decoder η^* obtained from the training set. Now, denote $\theta^+ = (\eta^*, \hat{\tau}(x))$, $\theta^* = (\eta^*, \phi^*)$, we define the Likelihood Regret (LR) of input data \mathbf{x} as

$$\text{LR}(\mathbf{x}) = \log p_{\theta^+}(\mathbf{x}) - \log p_{\theta^*}(\mathbf{x}). \quad (6)$$

Interpretation: In online learning, with the objective function f_{ξ} parameterized by ξ , and a sequence of observations x_1, \dots, x_T we obtain at time step T , the regret of a choice of parameter ξ^* measures how ‘sorry’ the learner is, in retrospect, not to have followed the predictions of the optimal hypothesis [33]:

$$R(T) = \frac{1}{T} \sum_{t=1}^T \max_{\xi_t} f_{\xi_t}(\mathbf{x}_t) - \frac{1}{T} \sum_{t=1}^T f_{\xi^*}(\mathbf{x}_t) \quad (7)$$

We borrow this idea of cumulative regret and propose the individual regret:

$$R(\mathbf{x}_{T+1}) = \max_{\xi} f_{\xi}(\mathbf{x}_{T+1}) - f_{\xi^*}(\mathbf{x}_{T+1}) \quad (8)$$

as a measure of the goodness of ξ^* in order to deal with new input \mathbf{x}_{T+1} .

Back to VAE model, for a given input, the Likelihood Regret is the log ratio of its likelihood obtained from the generative model (VAE) with optimal configuration of variational posterior distribution to its likelihood obtained from the VAE trained on training set. It measures the log likelihood improvement of the model configuration that maximizes the individual likelihood over the configuration that maximizes population likelihood. Intuitively, if the VAE is well trained on the training data distribution, given an in-distribution test sample, the encoder should output a good posterior configuration, and the improvement by replacing encoding posterior configuration with the optimal one should be small, hence resulting in low LR. In contrast, for an OOD test sample, since the model has not seen similar samples during training, the encoder is much less likely to output good posterior configuration, hence the LR could be large. Therefore, LR can serve as a good OOD detection score.

Implementation: The major component in evaluating LR is computing $\hat{\tau}(\mathbf{x})$ defined in (5). The log likelihood of the VAE is not easily computable, so we instead seek for the configuration $\tau(\mathbf{x})$ that maximizes the ELBO, just as is done in training the VAE. To estimate $\hat{\tau}(\mathbf{x})$, we fix the decoder η^* , and apply iterative optimization algorithms on τ with initialization $\tau^* = E_{\phi^*}(\mathbf{x})$ using $\mathcal{L}(\mathbf{x}; \eta^*, \tau)$ as the objective function until convergence. After obtaining $\hat{\tau}(\mathbf{x})$, we estimate the log likelihood $\log p_{\theta}(\mathbf{x}; \eta^*, \hat{\tau}(\mathbf{x}))$ by (2). Fixing the decoder parameter $\eta = \eta^*$ is crucial, otherwise it would overfit each single input and lose the information gathering from the training process. An alternative approach, instead of optimizing τ directly, is to optimize the parameters of the encoder given \mathbf{x} and $\eta = \eta^*$:

$$\phi^+(x) = \operatorname{argmax}_{\phi} \mathcal{L}(x; \eta^*, E_{\phi}(x)), \quad (9)$$

and compute likelihood regret based on (6) with $\theta^+ = (\eta^*, \phi^+(x))$. This one can be regarded as optimizing the posterior distribution restricted to the support of encoder.

5 Results

In this section, we conduct experiments to evaluate the performance of Likelihood Regret on OOD detection tasks on image datasets. For all experiments, we train VAEs with samples only from the training set of in-distribution data, and use test samples from different datasets to measure the OOD performances. Details regarding datasets and experimental settings can be found in Appendix A.

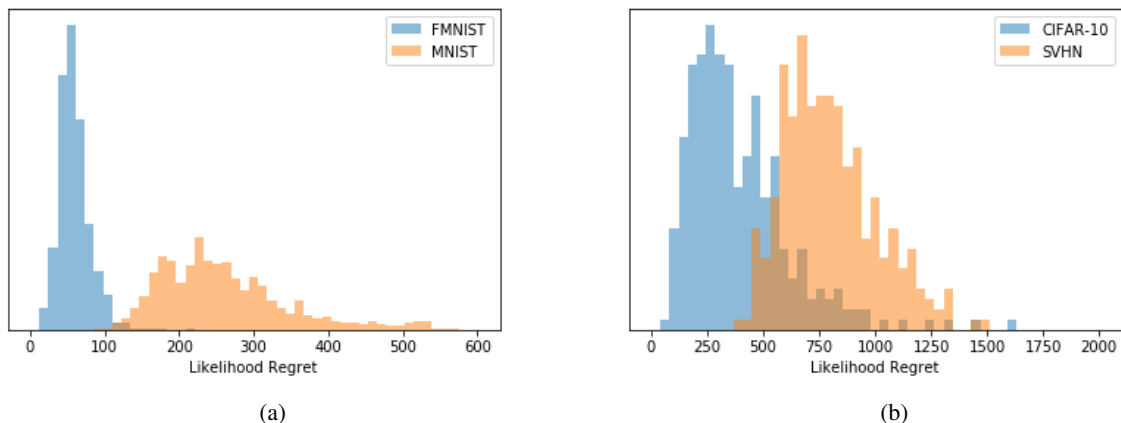


Figure 5.1: Histogram that compares the Likelihood Regret of test samples from (a): Fashion MNIST and MNIST on a VAE trained on Fashion MNIST, and (b): CIFAR-10 and SVHN on a VAE trained on CIFAR-10. Both experiments show that OOD samples tend to have higher LR, as expected.

We first follow the setting of [23] and conduct the following two experiments: (a) Fashion-MNIST as in-distribution and MNIST as OOD, and (b) CIFAR-10 as in-distribution and SVHN as OOD. We train VAEs on the training set of Fashion MNIST and CIFAR-10, and compute the Likelihood Regret for 1000 random samples from the test set of in-distribution data and corresponding OOD data. We plot the histograms of LR in Figure 5.1. Comparing Figure 2.1 with Figure 5.1, we observe that the VAE will assign higher likelihoods to OOD samples, while Likelihood Regret can largely correct such a likelihood misalignment. OOD samples typically have larger LR than in-distribution samples, which confirms the effectiveness of our OOD score.

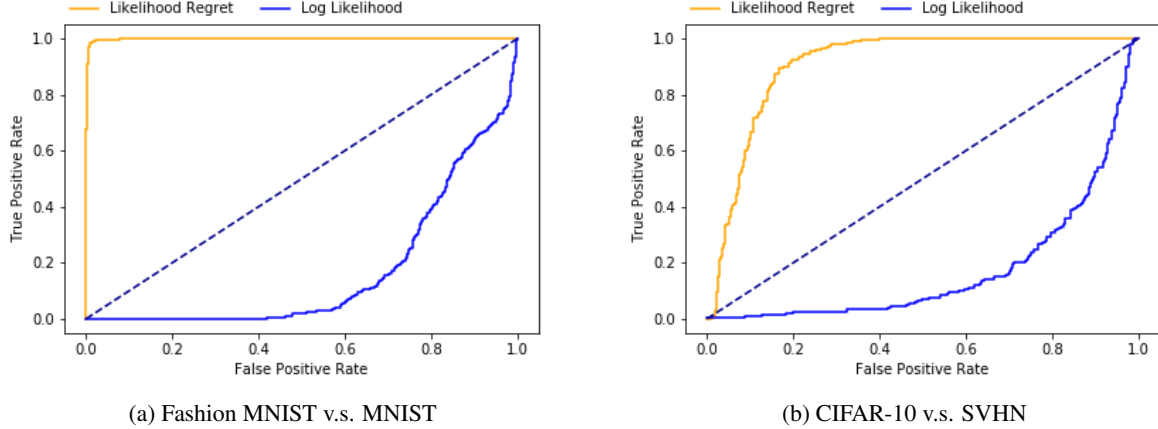


Figure 5.2: Comparing the ROC curves of using Likelihood Regret and Log Likelihood for OOD detection. On Fashion MNIST v.s. MNIST experiment, Likelihood Regret improves the AUC-ROC of OOD detection from 0.165 to 0.999. On CIFAR-10 v.s. SVHN experiment, Likelihood Regret improves the AUC-ROC of OOD detection from 0.161 to 0.866.

Like other OOD scores, Likelihood Regret needs a threshold when applied to the OOD detection task. The choice of a threshold depends on the particular application, and to quantitatively evaluate our method, we use Area Under The Curve-Receiver Operating Characteristics (AUCROC) as a metric. AUCROC is commonly used in OOD detection tasks [9], and it provides an effective performance summary across different score thresholds [6, 22]. In Figure 5.2, we plot the ROC curves for these two experiments, and results show that log likelihood is an extremely bad OOD detector as it achieves AUC-ROC much lower than 0.5 (random guessing), while LR obtains good OOD performances.

5.1 Quantitative Comparison with Other OOD Scores

After a simple verification of the effectiveness of our proposed OOD score, we carefully study its performances and compare it with competing methods. We use likelihood as a baseline, and include two implementations of input complexity adjusted score [32] as well as likelihood ratio with background model [29] in our comparison. Details of these methods and their implementation can be found in Appendix A.3. Using VAEs trained on Fashion MNIST and CIFAR-10, we test different OOD scores on a variety of datasets, and the AUCROC results are presented in Table 2. The choice of datasets largely follows [32], and in addition we create High Contrast (HC) Fashion MNIST and HC CIFAR-10 (See Appendix A.1). Note that we consider high contrast images from in-distribution datasets as a hard OOD task, especially on CIFAR-10, because they are visually similar to the in-distribution images and VAE assigns them similar likelihoods.

We make several observations from Table 2:

1. We confirm that likelihood is problematic in OOD detection. For example, VAE trained on CIFAR-10 not only assign significantly higher test likelihood on SVHN, but also on MNIST, Fashion MNIST and random constant images. The likelihood misalignment is reflected in an AUCROC value close to 0.
2. Likelihood Regret successfully corrects the misalignment of likelihood and obtains good OOD detection performances across all tasks, as the AUCROC values are close to the optimal value 1 on all experiments excepts for CIFAR-10 v.s CIFAR-100 and CIFAR-10 v.s CelebA. Note that these are the hard cases as all methods do not perform well. Strictly speaking, part of the CIFAR-100 images are in-distribution as they share class with CIFAR-10. we observe that optimizing the whole encoder works slightly better than only optimizing the mean and variance of variational posterior.
3. While competing methods also obtain good OOD detection performance on many tasks, all of them exhibit severe issues on specific tasks. For example, likelihood ratio with background model fails on the classic task of detecting SVHN from in-distribution CIFAR-10 (AUCROC only 0.27); both variants of input complexity adjusted likelihood fail almost completely on distinguishing between random uniform noise and CIFAR-10 (AUCROC close to 0). In addition, we also observe that the two variants of input complexity do not perform consistently across different tasks, making the choice between them difficult. These failure cases suggest that neither of these scores can be safely applied, at least for VAE models.

Overall speaking, we claim that LR achieves the best OOD detection performance, as it has very good AUCROC values without any failure case. Interestingly, the failure cases of competing methods do not exist in their papers where the scores are applied to Glow and PixelCNN. This is partly explained in Section 4.1. For example, on average, the difference of BPD returned by VAE is only 1.86 nats between CIFAR-10 and noise images, while for Glow and PixelCNN, the differences are 5.33 nats and 6.6 nats, respectively. However, the noise images have much larger complexity measurement than CIFAR-10, and the gap of complexity measurement will override the gap of likelihood, leading the input complexity adjusted score to make the wrong decision. Indeed, we observe that this happens sometimes, even for flow based models (see Appendix C). As for likelihood ratio with background model, this score heavily relies on the contrast between how well a single pixel is modeled by the main model and background model. However, VAEs are not designed for modeling each single pixel, and the bottleneck structure will “smooth out” the background, making the contrast with background model much less effective.

In summary, the experiments provide strong evidence that current state-of-the-art OOD scores for generative models may not be applicable to VAE, while our proposed score achieves good OOD detection results on a variety of tasks. To the best of our knowledge, Likelihood Regret is the only effective OOD score that can correct the likelihood misalignment of VAE.

	LR _E	LR _Z	Likelihood	Complexity (png)	Complexity (jp2)	Likelihood Ratio
MNIST	0.998	0.995	0.166	0.946	0.553	0.924
CIFAR-10	1	1	1	0.9315	0.999	0.968
SVHN	1	1	0.999	0.998	1	0.785
HC FMNIST	1	0.999	0.951	0.985	0.932	0.992
Noise	1	1	1	1	0.457	1
Constant	1	1	0.982	1	1	0.609

(a) Trained on Fashion MNIST

	LR _E	LR _Z	Likelihood	Complexity (png)	Complexity (jp2)	Likelihood Ratio
MNIST	1	0.997	0.008	0.994	0.988	0.792
FMNIST	1	0.995	0.062	0.997	0.992	0.691
SVHN	0.873	0.845	0.161	0.912	0.908	0.265
HC CIFAR-10	0.959	0.865	0.494	0.038	0.674	0.859
CIFAR-100	0.596	0.562	0.524	0.532	0.459	0.592
CelebA	0.723	0.690	0.493	0.651	0.535	0.447
Noise	1	0.959	1	0.032	0.054	1
Constant	0.998	0.896	0.007	1	1	0.470

(b) Trained on CIFAR-10

Table 2: Comparing LR and other OOD detection scores on different datasets. LR_E and LR_Z correspond to LR obtained from optimizing the encoder and only (μ_x, σ_x) , respectively.

5.2 Runtime

Our method requires 2 likelihood estimations and several optimization iterations for each testing image, which will make it slower than its competing methods. As a comparison, input complexity adjusted likelihood does not have computationally overhead, and likelihood ratio with background model needs 2 likelihood estimations. However, we observe that on average it takes less than 0.4s to optimize the encoder and less than 0.5s to optimize the latent distribution (which requires more iterations to converge, see Appendix A.2). The runtime for optimization is comparable to likelihood estimation (around 0.4s), so the computational overhead is acceptable.

5.3 Additional Results

To better illustrate Likelihood Regret, we compare the reconstruction of some test samples with trained VAE and optimized posterior distribution in Figure 5.3. Since as we show in Figure 2.2, the VAE can reconstruct both the in-distribution and out of distribution data very well, visually we cannot see obvious differences between reconstructed

images from VAE and from optimized $q_\phi(\mathbf{z}|\mathbf{x})$. However, we can still observe the improvements of reconstruction by the optimal $q_\phi(\mathbf{z}|\mathbf{x})$ in MNIST examples.

Some additional results are presented in the appendix. In Appendix B, we include OOD results of models trained on MNIST and SVHN for completeness. We observe that our method works well in these experiments, while competing OOD scores still exhibit some issues. In Appendix D, we show more qualitative examples of reconstruction on different test datasets. In Appendix E, we display some randomly generated samples from the VAEs. We obtain reasonable sample quality, indicating our VAEs model in-distribution data well.

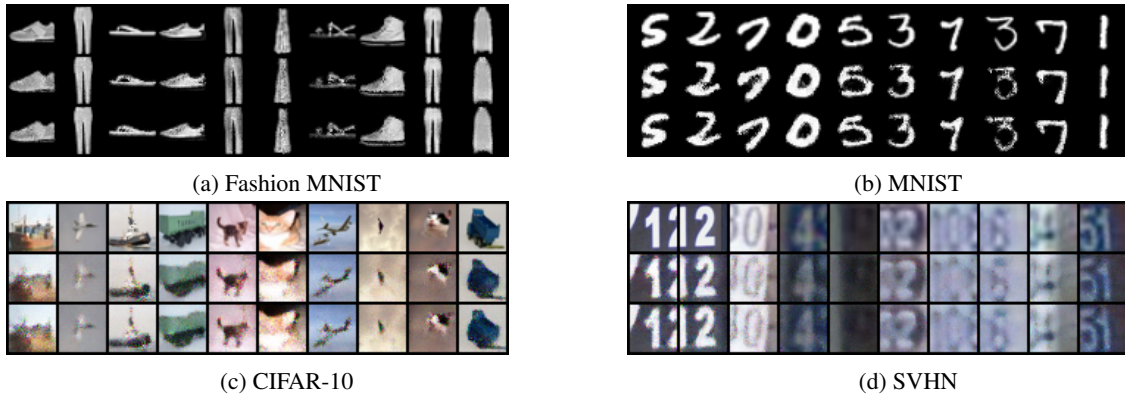


Figure 5.3: For each subfigure, the top row contains original images, the middle row contains the reconstruction from VAE, and the bottom row contains the reconstruction images with optimized encoder. **(a)**, **(b)** are obtained from VAE trained on Fshion MNIST. **(c)**, **(d)** are obtained from VAE trained on CIFAR-10.

6 Conclusion

In this paper, we carefully study the task of unsupervised out-of-distribution detection for VAEs. We evaluate some current state-of-the-art OOD scores on a set of experiments, and we conclude that their success on OOD detection for other probabilistic models cannot be easily transferred to VAEs, as they completely fail on some easy OOD detection tasks. We also try to provide clues to show that OOD detection is harder for VAE than for other generative models. To overcome the difficulty, we propose Likelihood Regret, an OOD score for VAEs that is effective on all tasks we evaluated. We hope this work can lead to further progress on OOD detection for probabilistic generative models and hopefully an OOD score that consistently performs well on all types of model and tasks.

References

- [1] Dario Amodei, Chris Olah, Jacob Steinhardt, Paul Christiano, John Schulman, and Dan Mané. Concrete problems in ai safety. *arXiv preprint arXiv:1606.06565*, 2016.
- [2] Lynton Ardizzone, Radek Mackowiak, Ullrich Köthe, and Carsten Rother. Exact information bottleneck with invertible neural networks: Getting the best of discriminative and generative modeling. *arXiv preprint arXiv:2001.06448*, 2020.
- [3] Yuri Burda, Roger Grosse, and Ruslan Salakhutdinov. Importance weighted autoencoders. *arXiv preprint arXiv:1509.00519*, 2015.
- [4] Hyunsun Choi, Eric Jang, and Alexander A Alemi. Waic, but why? generative ensembles for robust anomaly detection. *arXiv preprint arXiv:1810.01392*, 2018.
- [5] Terrance DeVries and Graham W Taylor. Learning confidence for out-of-distribution detection in neural networks. *arXiv preprint arXiv:1802.04865*, 2018.
- [6] Tom Fawcett. An introduction to roc analysis. *Pattern recognition letters*, 27(8):861–874, 2006.
- [7] Will Grathwohl, Kuan-Chieh Wang, Jörn-Henrik Jacobsen, David Duvenaud, Mohammad Norouzi, and Kevin Swersky. Your classifier is secretly an energy based model and you should treat it like one. *arXiv preprint arXiv:1912.03263*, 2019.
- [8] Karol Gregor, George Papamakarios, Frederic Besse, Lars Buesing, and Theophane Weber. Temporal difference variational auto-encoder. *arXiv preprint arXiv:186.03107*, 2018.
- [9] Dan Hendrycks and Kevin Gimpel. A baseline for detecting misclassified and out-of-distribution examples in neural networks. *arXiv preprint arXiv:1610.02136*, 2016.
- [10] Dan Hendrycks, Mantas Mazeika, and Thomas Dietterich. Deep anomaly detection with outlier exposure. *arXiv preprint arXiv:1812.04606*, 2018.
- [11] Diederik P Kingma and Max Welling. Auto-encoding variational bayes. *arXiv preprint arXiv:1312.6114*, 2013.
- [12] Durk P Kingma and Prafulla Dhariwal. Glow: Generative flow with invertible 1x1 convolutions. In *Advances in Neural Information Processing Systems*, pages 10215–10224, 2018.
- [13] Thomas N Kipf and Max Welling. Variational graph auto-encoders. *arXiv preprint arXiv:1611.07308*, 2016.
- [14] Alex Krizhevsky, Geoffrey Hinton, et al. Learning multiple layers of features from tiny images. 2009.
- [15] Balaji Lakshminarayanan, Alexander Pritzel, and Charles Blundell. Simple and scalable predictive uncertainty estimation using deep ensembles. In *Advances in neural information processing systems*, pages 6402–6413, 2017.
- [16] Yann LeCun, Corinna Cortes, and CJ Burges. Mnist handwritten digit database. 2010.
- [17] Dan Li, Dacheng Chen, Jonathan Goh, and See-Kiong Ng. Anomaly detection with generative adversarial networks for multivariate time series. *arXiv preprint arXiv:1809.04758*, 2018.
- [18] Dawen Liang, Rahul G Krishnan, Matthew D Hoffman, and Tony Jebara. Variational autoencoders for collaborative filtering. In *Proceedings of the 2018 World Wide Web Conference*, pages 689–698, 2018.
- [19] Ming-Yu Liu, Thomas Breuel, and Jan Kautz. Unsupervised image-to-image translation networks. In *Advances in neural information processing systems*, pages 700–708, 2017.
- [20] Ziwei Liu, Ping Luo, Xiaogang Wang, and Xiaoou Tang. Deep learning face attributes in the wild. In *Proceedings of the IEEE international conference on computer vision*, pages 3730–3738, 2015.
- [21] Lars Maaløe, Marco Fraccaro, Valentin Liévin, and Ole Winther. Biva: A very deep hierarchy of latent variables for generative modeling. In *Advances in neural information processing systems*, pages 6548–6558, 2019.
- [22] Charles E Metz. Basic principles of roc analysis. In *Seminars in nuclear medicine*, pages 283–298. WB Saunders, 1978.
- [23] Eric Nalisnick, Akihiro Matsukawa, Yee Whye Teh, Dilan Gorur, and Balaji Lakshminarayanan. Do deep generative models know what they don’t know? *arXiv preprint arXiv:1810.09136*, 2018.
- [24] Eric Nalisnick, Akihiro Matsukawa, Yee Whye Teh, and Balaji Lakshminarayanan. Detecting out-of-distribution inputs to deep generative models using a test for typicality. *arXiv preprint arXiv:1906.02994*, 2019.
- [25] Yuval Netzer, Tao Wang, Adam Coates, Alessandro Bissacco, Bo Wu, and Andrew Y. Ng. Reading digits in natural images with unsupervised feature learning. In *NIPS Workshop on Deep Learning and Unsupervised Feature Learning 2011*, 2011.

- [26] Anh Nguyen, Jason Yosinski, and Jeff Clune. Deep neural networks are easily fooled: High confidence predictions for unrecognizable images. In *Proceedings of the IEEE conference on computer vision and pattern recognition*, pages 427–436, 2015.
- [27] Aaron van den Oord, Sander Dieleman, Heiga Zen, Karen Simonyan, Oriol Vinyals, Alex Graves, Nal Kalchbrenner, Andrew Senior, and Koray Kavukcuoglu. Wavenet: A generative model for raw audio. *arXiv preprint arXiv:1609.03499*, 2016.
- [28] Alec Radford, Luke Metz, and Soumith Chintala. Unsupervised representation learning with deep convolutional generative adversarial networks. *arXiv preprint arXiv:1511.06434*, 2015.
- [29] Jie Ren, Peter J Liu, Emily Fertig, Jasper Snoek, Ryan Poplin, Mark Depristo, Joshua Dillon, and Balaji Lakshminarayanan. Likelihood ratios for out-of-distribution detection. In *Advances in Neural Information Processing Systems*, pages 14680–14691, 2019.
- [30] Danilo Jimenez Rezende, Shakir Mohamed, and Daan Wierstra. Stochastic backpropagation and approximate inference in deep generative models. *arXiv preprint arXiv:1401.4082*, 2014.
- [31] Tim Salimans, Andrej Karpathy, Xi Chen, and Diederik P Kingma. Pixelcnn++: Improving the pixelcnn with discretized logistic mixture likelihood and other modifications. *arXiv preprint arXiv:1701.05517*, 2017.
- [32] Joan Serra, David Álvarez, Vicenç Gómez, Olga Slizovskaia, José F Núñez, and Jordi Luque. Input complexity and out-of-distribution detection with likelihood-based generative models. *arXiv preprint arXiv:1909.11480*, 2019.
- [33] Shai Shalev-Shwartz and Yoram Singer. *Online learning: Theory, algorithms, and applications*. 2007.
- [34] Jiaming Song, Yang Song, and Stefano Ermon. Unsupervised out-of-distribution detection with batch normalization. *arXiv preprint arXiv:1910.09115*, 2019.
- [35] Aaron Van den Oord, Nal Kalchbrenner, Lasse Espeholt, Oriol Vinyals, Alex Graves, et al. Conditional image generation with pixelcnn decoders. In *Advances in neural information processing systems*, pages 4790–4798, 2016.
- [36] Han Xiao, Kashif Rasul, and Roland Vollgraf. Fashion-mnist: a novel image dataset for benchmarking machine learning algorithms. *arXiv preprint arXiv:1708.07747*, 2017.
- [37] Haowen Xu, Wenxiao Chen, Nengwen Zhao, Zeyan Li, Jiahao Bu, Zhihan Li, Ying Liu, Youjian Zhao, Dan Pei, Yang Feng, et al. Unsupervised anomaly detection via variational auto-encoder for seasonal kpis in web applications. In *Proceedings of the 2018 World Wide Web Conference*, pages 187–196, 2018.
- [38] Chunkai Zhang and Yingyang Chen. Time series anomaly detection with variational autoencoders. *arXiv preprint arXiv:1907.01702*, 2019.

A Experimental Settings

In this section, we introduce detailed settings of our experiments.

A.1 Datasets

We use several publicly available datasets in our experiments. These datasets include MNIST [16], Fashion-MNIST[36], CIFAR-10 and CIFAR-100[14], SVHN [25], and CelebA [20]. We also create two types of synthetic images: Noise and Constant. Noise images are random samples from $\text{Unif}[0, 1]$ distribution, and Constant images are images with constant value sampled from $\text{Unif}[0, 0.1]$. We also include high contrast Fashion MNIST and CIFAR-10, and they are obtained by randomly increase the contrast of original images by a factor between 2 and 2.5. Some examples of our created images are shown in Figure A.1.

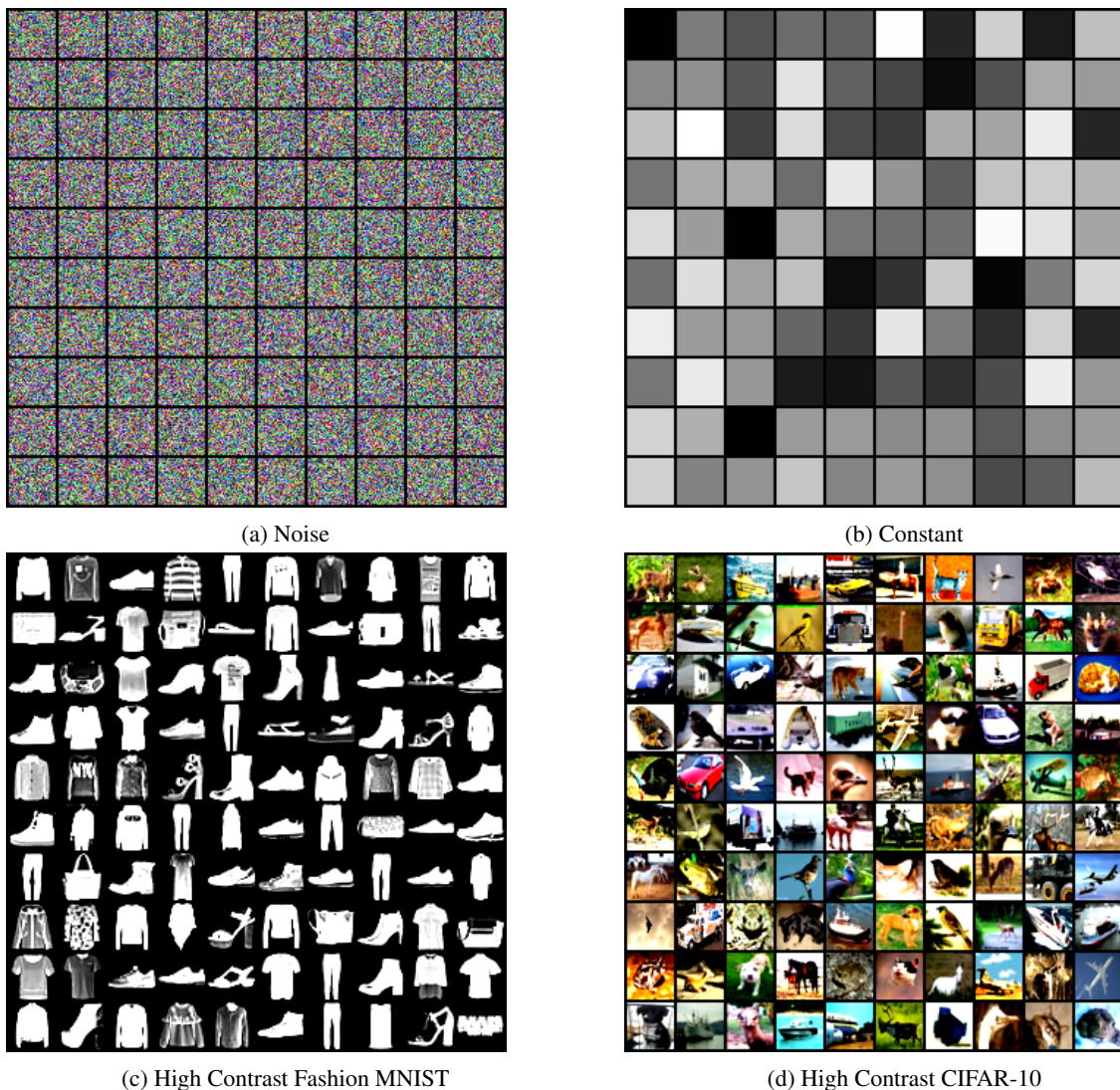


Figure A.1: Some examples of our created images used in experiments.

For most of our experiments, the VAE is trained on Fashion-MNIST and CIFAR-10, where we use the training partition of the datasets. For other datasets used for testing, we use a test partition if it is available, and use randomly sampled data if no predefined partition is available.

Encoder	Decoder
Input x	Input z , reshape to $nz \times 1 \times 1$
4×4 Conv _{nf} Stride 2, BN, ReLU	4×4 Deconv _{$4 \times nf$} Stride 1, BN, ReLU
4×4 Conv _{$2 \times nf$} Stride 2, BN, ReLU	4×4 Deconv _{$2 \times nf$} Stride 2, BN, ReLU
4×4 Conv _{$4 \times nf$} Stride 2, BN, ReLU	4×4 Deconv _{nf} Stride 2, BN, ReLU
4×4 Conv _{$2 \times nz$} Stride 1	4×4 Conv _{$256 \times nc$} Stride 2

Table 3: Network structure for VAE based on DCGAN. $nz = 100$ for all models. For VAE trained on Fashion MNIST, $nf = 32, nc = 1$; for VAE trained on CIFAR-10, $nf = 64, nc = 3$.

We resize images to spatial dimension 32×32 for all datasets. We trained VAE on Fashion MNIST using $32 \times 32 \times 1$ images, and when we test it on color images, we use only the first channel of the color image. When we use Fashion MNIST or MNIST images to test the VAE trained on CIFAR, we copy the channel three times to make them $32 \times 32 \times 3$.

A.2 Implementation Detail

The training and testing of our models largely follow the setting of [23]. In particular, we train VAEs with DCGAN [28] structure. We present the network structure in Table 3.

On Fashion MNIST we train the VAE for 100 epochs with constant learning rate $5e - 4$ using Adam optimizer and batch size 64. On CIFAR-10 we train the VAE for 200 epochs with constant learning rate $5e - 4$ using Adam optimizer and batch size 64. When computing Likelihood Regret, we have the choices of optimizing the whole encoder or only optimizing the mean and variance of posterior. For the former, we start with the trained encoder and optimize its parameters for 100 steps using Adam optimizer with learning rate $1e - 4$. For the later one, we start with the encoding mean and variance, and run optimization for 300 steps using Adam optimizer with learning rate $1e - 4$.

A.3 Implementing Competing Methods

Input complexity adjusted likelihood [32] is computed by subtracting the negative log likelihood with a measure of input’s complexity. The input complexity can be obtained from the length of binary strings that is returned by some lossless compression algorithms. We simply follow their work and use PNG compression and JPEG2000 compression implemented in OpenCV.

Likelihood ratio with background model [29] is computed by subtracting the log likelihood of the main model and the log likelihood of background model. The background model is trained by perturbing a proportion of randomly chosen pixels, where the perturbation is done by replacing the pixel value by a uniformly sampled random value between 0 and 255. One of the key hyper-parameters μ , is the percentage of pixels to be perturbed. The authors suggest to choose μ between 0.1 and 0.3. We do a simple grid search on $\{0.1, 0.2, 0.3\}$, and use the best one (0.3 for Fashion MNIST, and 0.2 for CIFAR-10). We trained the background VAE with the same setting of the main VAE, except that we apply $\lambda = 10 L_2$ weight decay as suggested by the authors.

B Results of Model Trained on SVHN

In Table 4, we include results of a set of simple experiments for VAE trained on SVHN. Note that in this case, likelihood itself works well on most tasks. We do not show results of VAE trained on MNIST because every method works nearly perfectly well. We observe that LR achieves good performances on all the tasks, while input complexity still have trouble with distinguishing noise from in-distribution data. In addition, its performance on SVHN v.s. CIFAR-10 lies far behind LR. As in Table 2, likelihood ratio has trouble on CIFAR-10 v.s. Constant. These failures suggest that competing OOD scores have systematical issues on VAE.

	LR _E	LR _Z	Likelihood	Complexity (png)	Complexity (jp2)	Likelihood Ratio
MNIST	1	1	1	1	1	1
FMNIST	1	0.999	1	1	1	0.928
CIFAR-10	0.924	0.842	0.982	0.524	0.608	0.936
Noise	1	1	1	0.235	0.105	1
Constant	1	1	0.213	1	1	0.136

Table 4: AUCROC for model trained on SVHN

C Issues with Input Complexity on Glow

In this section, we show the OOD results of input complexity adjusted likelihood for Glow trained on SVHN and MNIST. Note that this set of experiments are not performed by the authors of [32]. We use the same Glow structure used in [32], and train Glow on SVHN and MNIST dataset. We use input complexity adjusted likelihood to detect OOD samples from Fashion MNIST and CIFAR-10. Basically this is the reverse of the commonly conducted experiments. The AUCROC of MNIST v.s. Fashion MNIST is 0.633, and the AUCROC of SVHN v.s. CIFAR-10 is 0.518. Both results suggests that input complexity adjusted likelihood may not work in general, even on flow based model.

D More Reconstruction Examples

In this section, we present examples of reconstructed images in different datasets. See Figure D.1 and Figure D.2. We observe that VAE trained on CIFAR-10 can reconstruct images from multiple datasets very well.

E Randomly Generated Samples

We show some randomly generated samples from VAEs in Figure E.1. Although the samples are blurry and a bit noisy (due to the cross entropy loss), the semantics of samples suggest that our VAEs model the in-distribution data well.



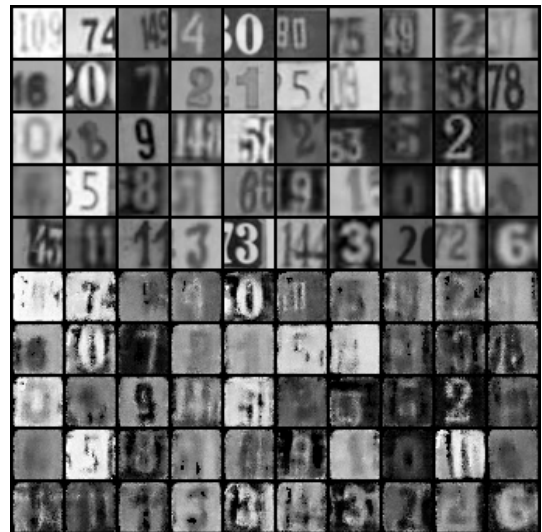
(a) Fashion MNIST



(b) MNIST



(c) CIFAR-10

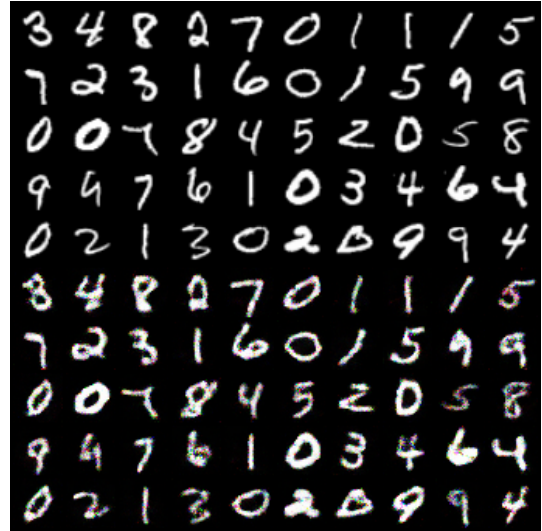


(d) SVHN

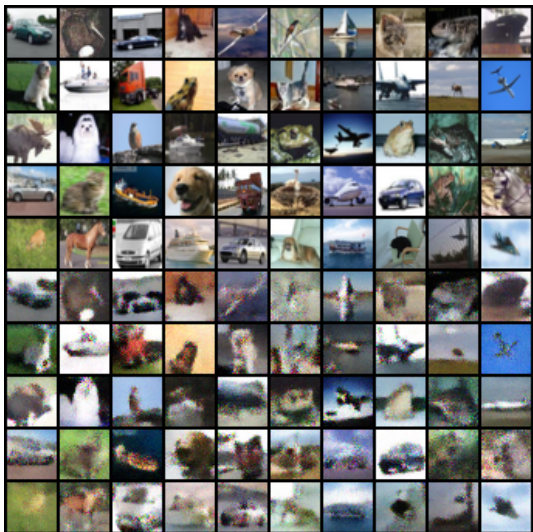
Figure D.1: Some examples of reconstructed images using VAE trained on Fashion MNIST. For each subfigure, the first 5 rows are original images and the last 5 rows are their corresponding reconstructions.



(a) Fashion MNIST



(b) MNIST



(c) CIFAR-10

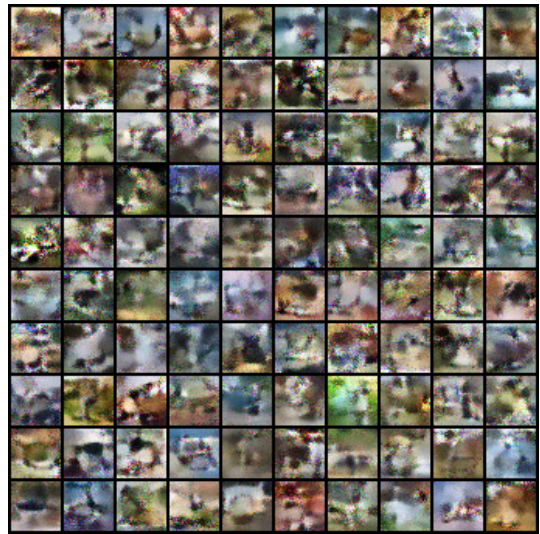


(d) SVHN

Figure D.2: Some examples of reconstructed images using VAE trained on CIFAR-10. For each subfigure, the first 5 rows are original images and the last 5 rows are their corresponding reconstructions.



(a) Fashion MNIST



(b) CIFAR

Figure E.1: Some examples of randomly generated samples.